International Journal of Thermodynamics (IJoT)
ISSN 1301-9724 / e-ISSN 2146-1511
www.ijoticat.com

Vol. 16 (No. 3), pp. 115-122, 2013
doi: 10.5541/ijot.516
Published online: Sept. 01, 2013

Numerical Investigation of Heat and Mass Transport and Surface Condensation due to Food Respiration and Transpiration in a Refrigerated Space

Serdar Kocatürk[1]*, A. Nilüfer Eğrican[2]

[1]Arçelik A.Ş. R&D Center 34950 Tuzla İstanbul - TURKIYE
[2]Suntek International 34865 Kartal İstanbul - TURKIYE
E-mail: [1]serdar.kocaturk@arcelik.com; [2]egrican@gmail.com

Abstract

Food load and air-flow area within a refrigerated space having one air inlet and one air outlet have been taken as two separate control volumes interacting with each other at their boundaries. In the lower control volume, stored vegetable products have been located and heat and mass transfer due to respiration and transpiration of these products have been modeled for determining boundary conditions of the upper control volume, in which heat and mass transport within the air circulation above the products have been modeled and numerically investigated. Upper surface temperature of the said upper control volume has been compared with the dew point temperature, and condensation heat and mass fluxes through the surface have been calculated at the upper boundary. Time-dependent heat and mass transport equations of the control volume have been simultaneously solved together. An implicit finite difference approach has been applied for the numerical solution of transport equations. Fortran programming language has been used to develop the numerical model. As a result, temperature and humidity ratio distribution, the amount of vapor transpiration from food products, and the amount of condensation on the underside of the upper surface due to heat-and-mass transport and transpiration characteristics of the products have been time-dependently calculated for two different dimensions of the air inlet.

Keywords: *Surface condensation; food respiration; transpiration; humidity; moisture loss; water vapor; mass concentration; finite difference.*

1. Introduction

Water vapor produced by respiration and transpiration of food products such as fruit and vegetables in a refrigerated space, causes the increase of humidity ratio in the space. Due to heat-and-mass transport characteristics (air circulation, temperature, humidity ratio) of humid air and food products, a specific relative humidity is obtained at the operating temperature of refrigerated space. Ideal relative humidity values for storing a plurality of fruits and vegetables is ~90% at the temperature intervals of 2-10^{o}C (ASHRAE, 2006). At this high relative humidity conditions, water vapor condenses on surfaces cooled under dew-point temperatures of humid air conditions in the space.

In a numerical investigation of heat and mass transfer during refrigeration of fruit and vegetables, a computational algorithm for heat loads and moisture loss of refrigerated fruits and vegetables had been developed (Becker et al., 1996a, 1996b).

Moisture loss from fresh food surface has been defined as transpiration. Three stages of transpiration are; moisture transport through the surface, evaporation of moisture from the surface, and convective mass transfer from surface to ambient (ASHRAE, 2006; Becker et al., 1996). The main factor contributing to said mass transfer is the water vapor concentration difference between surface and air. This concentration difference can be associated with the difference between vapor saturation pressure on the surface and partial vapor pressure in humid air (ASHRAE, 2006). Mass flux m due to transpiration from unit surface of food has been given as Eq. (1), in which k_t is the transpiration coefficient, P_s is the water vapor saturation pressure on the food surface, and P_v is the partial vapor pressure in the air.

$$m'' = k_t \cdot (P_s - P_v) \tag{1}$$

Respiration of fruits and vegetables is an exothermic chemical reaction of which CO_2, water vapor, and respiration heat are the outputs. Respiration heat dissipated with 1 mg CO_2 has been 10.7 kJ, and respiration heat produced by unit mass of food has been expressed with respect to CO_2 production rate as given in Eq.(3) (Çengel and Boles, 2000; ASHRAE, 2006; Becker et al., 1996).

$$C_6H_{12}O_6 + 6O_2 \rightarrow 6CO_2 + 6H_2O + 2667 \text{ kJ} \tag{2}$$

$$q''_{resp.}\,[J/kgh] = 10,7 \cdot \dot{m}_{CO2} \tag{3}$$

CO_2 production rate during respiration is given in Eq. (4), in which f and g are respiration coefficients differing with respect to the type of food. These respiration coefficients for different fruits and vegetables have been given in literature according to USDA (ASHRAE, 2006; Becker et al., 1996).

$$\dot{m}_{CO2} = f \cdot \left(\frac{9 \cdot T_m}{5} + 32 \right)^g \quad \text{[mg/(kg.h)]} \tag{4}$$

A general mathematical modeling methodology had been developed for design of refrigerated fruit-and-

*Corresponding Author

vegetable packages (Taner et al., 2002). By using the developed mathematical model, they evaluated product refrigeration rates, moisture loss, local relative humidity levels, and moisture contents of the packaging material for various fruits-and-vegetables and packaging materials (Taner et al., 2002a, 2002b, 2002c).

Heat and mass transfer due to condensation of humid air in cooled open cavities in the case of natural convection in vertical direction had been experimentally investigated (Terrell and Newell, 2007). Boundary layer heat and mass transfer in a forced flow of humid air with steam condensation on an upward surface had been numerically studied (Volchlov et al., 2004). In the study, that laminar film condensation on a finite-size horizontal wavy disk had been investigated, they determined that heat transfer coefficient and film thickness had been functions of Pr, Ja, Ra parameters and dimensions of the wavy structure (Yang et al., 1997). Film condensation on a horizontal surface having a thick porous layer had been numerically modeled with a boundary layer approach (Wang et al., 2006; White, 2000).

Some of the prior art related with heat and mass transfer about transpiration and respiration of fruits and vegetables have been presented above. Separate from food respiration and transpiration, surface condensation had generally been investigated for the cases of natural convection on vertical surface or forced convection on horizontal surface in prior art. In the case of fruit and vegetable refrigeration in a closed space, condensation on the surfaces having temperature below dew point temperature will perform due to respiration and transpiration of the food. In that case, surface condensation should be related with the heat-and-mass transfer calculations on food respiration and transpiration. So that, heat and mass transport equations for both refrigerated space and food load are needed to be solved simultaneously with interacting boundaries about condensation, transpiration and respiration. In this study; heat-and-mass transport and surface condensation due to food respiration and transpiration in the refrigerated space have been investigated. Physical and mathematical modeling details in the study are given in further sections.

2. Analysis and Modeling Methodology

In order to determine velocity profiles necessary for heat and mass transport equations, momentum equation for homogenous air – vapor mixture has been solved firstly. Then heat and mass transport equations both for the upper and lower control volumes have been solved simultaneously. Food products have been considered to be put in the refrigerated space at ambient temperature and time-dependent solution until the products have been cooled to the storing temperature has been performed. Initial conditions of air for the time-dependent solution has been determined by the steady-state solution of heat and mass transport equations for the empty space before product loading.

2.1 Physical Model and Boundary Conditions

Refrigerated space having at least one air inlet and one air outlet and having vegetables located for cool storing, has been modeled as two control volumes interacting with each other. A schematic view of the physical model is given in Figure 1. In the control volume CV2, stored vegetable products have been located and heat and mass transfer due to respiration and transpiration of these products have been modeled for determining boundary conditions of the upper control volume CV1. In the control volume CV1, heat and mass transport within the air circulation above the products have been modeled. Surface temperatures have been taken as boundary conditions at the surfaces. Heat flux due to food respiration and water vapor mass flux due to food transpiration through the interface between two control volumes have been taken as lower boundary conditions of CV1 control volume in the solution of relating heat and mass transport equations. Upper surface temperature of CV1 has been compared with the dew point temperature, and in the case of having a temperature below dew point temperature, condensation heat and mass fluxes through the surface have been taken as upper boundary condition with the surface temperature. Air flow rate through inlet opening has also been taken as boundary condition. Dimension descriptions of the control volumes are given in Figure 2, and said dimension values are given with the boundary condition values in Table 1.

2.2 Mathematical Modeling of the Upper Control Volume CV1

Continuity and Momentum Equations:

General form of the Continuity Equation is given in Eq. (5) where ρ_m [kg/m^3] is the density of humid air constituting from the mixture of dry air and water vapor. Because of low velocity values, the effect of velocity difference of the two ingredients of the mixture on the total velocity profile is going to be relatively low. So for the practical solution of momentum equations in order to determine velocity profiles used in heat and mass transport

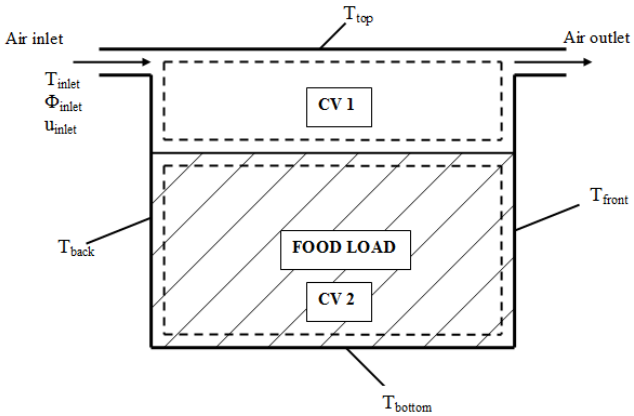

Figure 1. Scheme of the physical model.

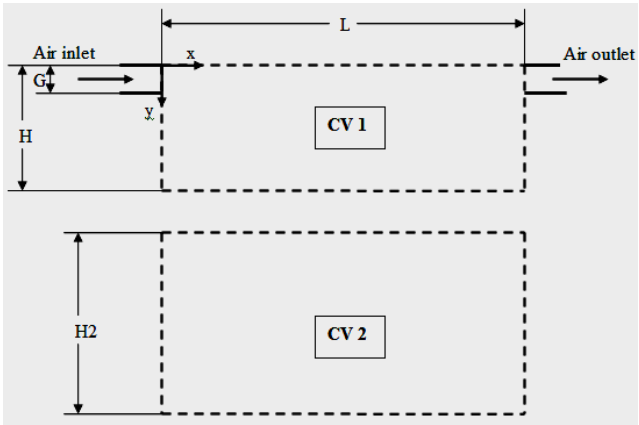

Figure 2. Dimension descriptions of the control volumes.

Table 1. Dimensions and boundary conditions.

Air Inlet Conditions			
Temperature	T_{inlet}	2	°C
Relative Humidity	Φ_{inlet}	30	%
Velocity	u_{inlet}	0.017	m/s
Surface Temperatures			
Top	T_{top}	3	°C
Bottom	T_{bottom}	8	°C
Front	T_{front}	6	°C
Back	T_{back}	7	°C
Dimensions			
Length	L	260	mm
Height of CV1"	H	80	mm
Height of CV2"	H2	150	mm
Height of Air Inlet	G	18	mm
Depth	DR	275	mm

equations, homogenous flow approach has been applied instead of separate flow approach. Momentum equations have been written and aimed to be solved in steady-state regime. Hence, continuity equation, momentum equations in x direction and y direction have been as given in Eqs. (6)-(8) respectively. Gravity effects have been neglected (White, 1991; Mills, 2000).

$$\frac{\partial \rho_m}{\partial t} + div\left(\rho_m \cdot \vec{V}\right) = 0 \tag{5}$$

$$\frac{\partial u}{\partial x} + \frac{\partial v}{\partial y} = 0 \tag{6}$$

$$u \cdot \frac{\partial u}{\partial x} + v \cdot \frac{\partial u}{\partial y} = -\frac{1}{\rho_m} \cdot \frac{\partial P}{\partial x} + \upsilon_m \cdot \left(\frac{\partial^2 u}{\partial x^2} + \frac{\partial^2 u}{\partial y^2} \right) \tag{7}$$

$$u \cdot \frac{\partial v}{\partial x} + v \cdot \frac{\partial v}{\partial y} = -\frac{1}{\rho_m} \cdot \frac{\partial P}{\partial y} + \upsilon_m \cdot \left(\frac{\partial^2 v}{\partial x^2} + \frac{\partial^2 v}{\partial y^2} \right) \tag{8}$$

Pressure gradient in the x direction has been taken as $\frac{\partial P}{\partial x} \approx \frac{\Delta P}{L}$ where ΔP is the pressure loss experimentally measured along the length L for a similar geometry in the same velocity conditions (ΔP = 0.0033 Pa). Because the air inlet and outlet are in the same x direction, pressure gradient in the y direction has been neglected. Velocity at the air outlet has been determined from the solution of momentum equations. Boundary conditions for the solution of $u(x,y)$ and $v(x,y)$ in the momentum equations are given in Eq. (9)-(12).

$$u(x,0) = 0 \;\; ; \;\; v(x,0) = 0 \tag{9}$$

$$u(0,y) \prod_{y=0}^{G} = U_{inlet} \;\; ; \;\; u(0,y) \prod_{y=G}^{H} = 0 \;\; ; \;\; v(0,y) = 0 \tag{10}$$

$$u(L,y) \prod_{y=0}^{G} = u(L-\Delta x, y) \prod_{y=0}^{G} ; u(L,y) \prod_{y=G}^{H} = 0 ; v(L,y) = 0 \tag{11}$$

$$u(x,H) = 0 \;\; ; \;\; v(x,H) = 0 \tag{12}$$

Implicit Crank-Nicolson finite difference numerical approach (Anderson, 1995) has been applied for numerical discretization of the differential equations, and discrete penta-diagonal matrix equations have been numerically solved by Gauss-Seidel iteration.

Heat and Mass Transport Equations:

Two-dimensional, time-dependent form of the energy equation is given in Eq. (13)"; where k [W/m.K] is the thermal conductivity, c_p [J/kg.K] is the specific heat, ρ_m [kg/m^3] is the density of humid air, and $\alpha_T = \frac{k}{\rho \cdot c_p}$ [m^2/s] is the thermal diffusivity. Similarly; two-dimensional, time-dependent form of the Mass Transport Equation is given in Eq. (14)"; where D_{va} [m^2/s] is the binary diffusion coefficient between air and water vapor in humid air, d_v [kg/m^3] is the mass concentration of water vapor in humid air.

$$\frac{\partial T}{\partial t} + u \cdot \frac{\partial T}{\partial x} + v \cdot \frac{\partial T}{\partial y} = \alpha_T \cdot \left(\frac{\partial^2 T}{\partial x^2} + \frac{\partial^2 T}{\partial y^2} \right) \tag{13}$$

$$\frac{\partial d_v}{\partial t} + u \cdot \frac{\partial d_v}{\partial x} + v \cdot \frac{\partial d_v}{\partial y} = D_{va} \cdot \left(\frac{\partial^2 d_v}{\partial x^2} + \frac{\partial^2 d_v}{\partial y^2} \right) \tag{14}$$

After the solution of momentum equations in order to determine velocity profiles necessary for heat and mass transport equations, initial conditions of air for the time-dependent solution have been determined by the steady-state solution of heat and mass transport equations for the empty space before product loading. For the steady-state solution of energy equation, surface temperatures and air inlet conditions given in Table 1 have been taken as boundary conditions. Similarly, no mass transfer at the surfaces has been taken as boundary conditions for the solution of steady-state mass transport equation. Then food products have been considered to be put in the refrigerated space at ambient temperature and time-dependent solution of the transport equations for both control volumes until the products have been cooled to the storing temperature has been performed simultaneously. Modeling equations for CV2 are explained in further sub-section.

Initial and boundary conditions for the solution of $T(x,y,t)$ in the Energy Equation Eq. (13) are given in Eq. (15)-(19).

$$T(x,y,0) = T_o(x,y) \tag{15}$$

$$T(x,0,t) = T_{top} \tag{16}$$

$$T(0,y,t) \prod_{y=0}^{G} = T_{inlet} \;\; ; \;\; T(0,y,t) \prod_{y=G}^{H} = T_{back} \tag{17}$$

$$T(L,y,t) \prod_{y=0}^{G} = T(L-\Delta x, y) \prod_{y=0}^{G} ; T(L,y,t) \prod_{y=G}^{H} = T_{front} \tag{18}$$

$$k_m \cdot \frac{\partial T(x,H,t)}{\partial y} = h \cdot \left[T_g(x,H,t) - T(x,H,t) \right] \tag{19}$$

Boundary condition for the top surface having the coldest temperature within all surfaces and having the possibility of surface condensation on it, has been taken as a constant surface temperature T_{top}. If the surface temperature T_{top} is below the dew point temperature T_{dew}, surface condensation will occur with respect to the vapor concentration difference between the concentration values at dew-point conditions and saturation conditions at the top surface temperature as seen in Eq. (21). Dew-point temperature T_{dew} is the saturation temperature at the partial water vapor pressure in humid air. T_{dew} for each Δx has been calculated due to the relations in Eq. (20) given in the literature (Olivieri and Singh, 1996), and mass concentration of water vapor and relative humidity calculated from the solution of mass transport equation.

$$\begin{aligned} &\alpha = AT^2 + BT + C + DT^{-1},\ T\left[\mathrm{K}\right] \text{ and } P_{sat.} = 1000\exp(\alpha),\ \mathrm{P}\left[\mathrm{Pa}\right] \\ &T_{sat.} = E\beta^4 + F\beta^3 + G\beta^2 + H\beta + K,\ \left[\mathrm{K}\right] \text{ and } \beta = \ln(P_v),\ \mathrm{P}\left[\mathrm{Pa}\right] \end{aligned} \quad [20]$$

$$\left[m''_{\text{cond.}}(t)\right]_{\Delta x} = \left[(d_v)_{\text{dew}} - (d_v)_{\text{surf.}}\right]_{\Delta x} \cdot H/\Delta t \quad (21)$$

Total density of a gas mixture such as humid air is the rate of total mass of the mixture to the total volume. So that, total mixture density of humid air can be expressed as the sum of mass concentrations of water vapor and dry air in the humid air mixture as given in Eq. (22) (Incropera et al., 2007; Mills, 2000).

In the literature (ASHRAE, 2006; Becker et al., 1996), expressions for the total density of humid air are given due to dry air and water vapor mole fractions in the mixture. Besides, humidity ratio ω can be expressed as the ratio of mass concentration of water vapor to the mass concentration of dry air in the mixture (Olivieri and Singh, 1996; ASHRAE, 2006; Mills,2000). Hence, relation between water vapor mass concentration in the humid air and psychrometric humidity ratio can be expressed as given in Eq. (23). After the solution of Mass Transport Equation Eq. (14) for the mass concentration of water vapor in the humid air, humidity ratio distribution in the control volume has been evaluated via using the relation given in Eq. (23). Then relative humidity distribution has also been evaluated by psychrometric relations (Olivieri and Singh, 1996) between humidity ratio, temperature and relative humidity. Temperature values needed for the solution of these relations have been calculated from the solution of Energy Equation Eq. (13).

For the lower boundary, convective heat transfer between the vegetable goods' surface and circulating humid air has been taken as the boundary condition. Vegetable goods' temperature T_g has been solved from the energy equation written for the food load in CV2. Convective heat transfer coefficient h can be calculated from *Nu-Re-Pr* relations given in literature. In this study, h has been taken constant as 5 W/m^{2}K for preliminary calculations.

Initial and boundary conditions for the solution of $d_v(x,y,t)$ in the Mass Transport Equation Eq. (14) are given in Eq. (24)-(28). Mass flux due to surface condensation has been taken as upper boundary condition as given in Eq. (25). No mass transfer on the surfaces has been taken as boundary conditions on back and front surfaces.

$$\rho_m = \frac{m_{\text{TOTAL}}}{V} = \frac{m_v}{V} + \frac{m_a}{V} = d_v + d_a \quad \left[\mathrm{kg/m^3}\right] \quad (22)$$

$$\begin{aligned} \rho_m = d_v + d_a \ &\Rightarrow \ \frac{218{,}84}{T_a}\cdot\left(\frac{1+\omega}{0{,}62198+\omega}\right) = d_v + \frac{d_v}{\omega} \\ &\Rightarrow \ d_v = \frac{218{,}84}{T_a}\cdot\left(\frac{\omega}{0{,}62198+\omega}\right) \end{aligned} \quad (23)$$

$$d_v(x,y,0) = d_{vo}(x,y) \quad (24)$$

$$D_{va}\cdot\frac{\partial d_v(x,0,t)}{\partial y} = \left[m''_{cond.}(t)\right]_{\Delta x} \quad (25)$$

$$\begin{aligned} &d_v(0,y,t)\Big|_{y=0}^{G} = (d_v)_{\text{inlet}} = \frac{218{,}84}{T_a}\cdot\left(\frac{\omega_{\text{inlet}}}{0{,}62198+\omega_{\text{inlet}}}\right) \\ &\frac{\partial d_v(0,y,t)}{\partial x}\Big|_{y=G}^{H} = 0 \end{aligned} \quad (26)$$

$$\begin{aligned} &d_v(L,y,t)\Big|_{y=0}^{G} = d_v(L-\Delta x,y)\Big|_{y=0}^{G} \\ &\frac{\partial d_v(L,y,t)}{\partial x}\Big|_{y=G}^{H} = 0 \end{aligned} \quad (27)$$

$$D_{va}\cdot\frac{\partial d_v(x,H,t)}{\partial y} = m''_{\text{transp.}}(t) \quad (28)$$

For the lower boundary, mass flux due to the transpiration of vegetable goods has been taken as the boundary condition as given in Eq. (28). Mass flux $m''_{transp.}$ due to transpiration from unit surface of food has been calculated as given in Eq. (37). Transpiration coefficient has been taken approximately equal to the diffusive surface mass transfer coefficient of the vegetable as $k_t \approx k_s$. Diffusive surface mass transfer coefficient k_s [g/m^2.s.Pa], experimentally determined for various fruits and vegetables by Chau et al. (1987) and Gan & Woods (1989), are given in literature (ASHRAE, 2006). Water vapor saturation pressure P_s on the food surface has been calculated for vegetable surface temperatures T_g that have been determined from the solution of the energy equation written for vegetable goods in CV2. Partial vapor pressure P_v in the air has been calculated according to the temperature and relative humidity distributions in the control volume. Saturation and partial vapor pressures have been calculated by using the mathematical relations given in Eq. (20).

Implicit Crank-Nicolson finite difference numerical approach has been applied for numerical discretization of the differential equations, and discrete penta-diagonal matrix equations have been numerically solved by Gauss-Seidel iteration. Penta-diagonal matrix equations derived from numerical discretization of Energy Equation and Mass Transport Equation are given in Eq. (29) and Eq. (30) respectively. In these equations; $c_x = u\cdot\frac{\Delta t}{\Delta x}$ and $c_y = v\cdot\frac{\Delta t}{\Delta y}$ are dimensionless Courant numbers (Anderson, 1995), $d_x = \alpha\cdot\frac{\Delta t}{(\Delta x)^2}$ and $d_y = \alpha\cdot\frac{\Delta t}{(\Delta y)^2}$ are dimensionless thermal diffusivity numbers for energy equations, $d_x = D_{va}\cdot\frac{\Delta t}{(\Delta x)^2}$ and $d_y = D_{va}\cdot\frac{\Delta t}{(\Delta y)^2}$ are dimensionless mass diffusivity numbers for mass transport equations (Anderson, 1995). n

is the known previous time interval, and n+1 is the current unknown time interval, unknowns of which constitute a penta-diagonal matrix equation to be solved.

$$(c_x - 2d_x)\cdot T_{i+1,j}^{n+1} - (c_x + 2d_x)\cdot T_{i-1,j}^{n+1} + (c_y - 2d_y)\cdot T_{i,j+1}^{n+1} - (c_y + 2d_y)\cdot T_{i,j-1}^{n+1} + 4\cdot(1 + d_x + d_y)\cdot T_{i,j}^{n+1} = f(T^n) \quad (29)$$

$$(c_x - 2d_x)\cdot (d_v)_{i+1,j}^{n+1} - (c_x + 2d_x)\cdot (d_v)_{i-1,j}^{n+1} + (c_y - 2d_y)\cdot (d_v)_{i,j+1}^{n+1} - (c_y + 2d_y)\cdot (d_v)_{i,j-1}^{n+1} + 4\cdot(1 + d_x + d_y)\cdot (d_v)_{i,j}^{n+1} = f\left[(d_v)^n\right] \quad (30)$$

The control volume has been divided into 261 nodes in the x-direction, and 81 nodes in y-direction, so that numerical discretization interval between each computational nodes have been $\Delta x = \Delta y = 1$ mm. Computational time interval has been taken as $\Delta t = 0.1$ s. FORTRAN Programming Language has been used for the solution of said computational equations and iteration runs.

2.3 Mathematical Modeling of the Lower Control Volume CV2

In the control volume CV2, stored vegetable goods have been located and heat and mass transfer due to respiration and transpiration of these products have been modeled for determining boundary conditions of the upper control volume CV1.

Two-dimensional, time-dependent form of the Energy Equation for the food load is given in Eq. (31)"; where $q_{resp.}^{"}$ is the heat of respiration given in Eq. (3), and $m_{transp.}^{"} \cdot h_{fg}$ is the evaporative cooling effect due to transpiration from food surface. $m_{transp.}^{"}$ is calculated with $\Lambda\ \left[kg/m^2\right]$ which denotes the weight of food product per surface area for mass transfer. The related expression is given in Eq. (37). Λ has been determined by rating the weight of cucumber to the surface area calculated from measured diameters at 7 different equal intervals through the length of cucumber. These measurements have been performed for a reasonable number of Antalya cucumbers and average Λ has been determined to be 7.6 kg/m^2.

Initial and boundary conditions for the solution of $T_g(x,y,t)$ in the Energy Equation Eq. (31) are given in Eq. (32)-(36). For the upper boundary, convective heat transfer between the vegetable goods' surface and circulating humid air has been taken as the boundary condition. Air temperature has been solved from the energy equation written for CV1. Other boundary conditions have been taken as the surface temperatures given in Table 1. Vegetable goods have been considered to be put in the refrigerated space at $T_{amb.}$=290 K ambient temperature.

$$\frac{\partial T_g}{\partial t} = \alpha_{Tg}\cdot\left(\frac{\partial^2 T_g}{\partial x^2} + \frac{\partial^2 T_g}{\partial y^2}\right) + \frac{q_{resp.}^{"}}{(c_p)_g} - \frac{m_{transp.}^{"}\cdot h_{fg}}{(c_p)_g} \quad (31)$$

$$T_g(x, y, 0) = T_{amb.} \quad (32)$$

$$k_m \cdot \frac{\partial T_g(x,H,t)}{\partial y} = h\cdot\left[T_g(x,H,t) - T(x,H,t)\right] \quad (33)$$

$$T_g(0, y, t) = T_{back} \quad (34)$$

$$T_g(L, y, t) = T_{front} \quad (35)$$

$$T_g(x,(H+H2),t) = T_{bottom} \quad (36)$$

$$m_{transp.}^{"} = k_t\cdot(P_s - P_v)/\Lambda \quad (37)$$

Heat and mass transport equations for the upper control volume CV1, and energy equation for the food load in the control volume CV2 have been solved simultaneously with interacting boundaries, and time-dependent solution until the products have been cooled to the storing temperature has been performed. Numerical discretization interval between each computational node has been $\Delta x = \Delta y = 1$ mm. Computational time interval has been taken as $\Delta t = 0.1$ s.

In order to satisfy reasonable computation times and stability for convergence, the course of the Courant numbers c_x and c_y especially during cooling down transient regime have been numerically followed. In order to hinder divergence, the value of computational time interval Δt has been defined small enough to take possible instantaneous increase of Courant numbers under control. For convergence, satisfaction of the criteria given in Eq. (38) has been controlled.

As the result of numerical simultaneous solution of transport equations for the two control volumes; temperature and humidity ratio distribution of the circulating humid air, temperature distribution within the food load, the amount of vapor transpiration from food products, and the amount of condensation on the underside of the upper surface due to heat-and-mass transport and transpiration characteristics of the products have been time-dependently determined.

$$\frac{\left|(d_v)_{i,j}^{n+1} - (d_v)_{i,j}^{n}\right|}{\left|(d_v)_{i,j}^{n+1}\right|} \le 10^{-5}\ ;\ \frac{\left|T_{i,j}^{n+1} - T_{i,j}^{n}\right|}{\left|T_{i,j}^{n+1}\right|} \le 10^{-5}\ ;\ \frac{\left|(T_g)_{i,j}^{n+1} - (T_g)_{i,j}^{n}\right|}{\left|(T_g)_{i,j}^{n+1}\right|} \le 10^{-5} \quad (38)$$

3. Results and Discussion

For the case of air inlet cross-section height being G=18 mm, volume air flow rate at the inlet has been ~0.084 L/s. Numerical calculations were performed for cucumber being as the food load.

Air temperature distribution in the upper control volume CV1 and food load temperature distribution in the lower control volume CV2 after 10^6 iterations (1666 minutes) are given in Figure 3 and Figure 4 respectively. Average temperature of the food load and maximum temperature near to the central region of the load have been 9.4^{o}C and 11.6^{o}C respectively, while the average air temperature has been 5.2^{o}C. In these prior analyses, food load was assumed as fulfilling the whole loading area, and energy equation for the food load has been numerically solved in rectangular coordinates. Heat transport through the load has been by heat conduction, except convection heat transfer boundary condition between air and food surface at the top. For future analyses, food load will be able to be modeled with porosity, and specific coordinates for the food load geometry. In that case, food load temperatures for the same number of iterations will be lower.

Mass concentration of water vapor in humid air, which has been calculated from the solution of mass transport equation, after 10^6 iterations is given in Figure 5. Relative humidity and humidity ratio distributions that have been

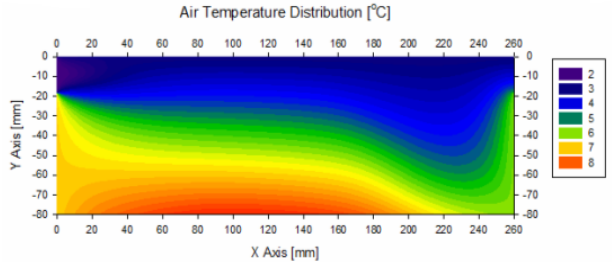

Figure 3. Air temperature distribution in the case of G=18mm after 10^6 iterations. (Figure is in color in the on-line version of the paper).

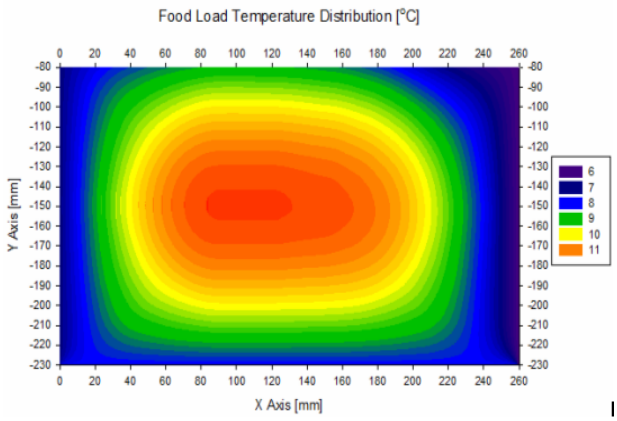

Figure 4. Food load temperature distribution in the case of G=18mm after 10^6 iterations. (Figure is in color in the on-line version of the paper).

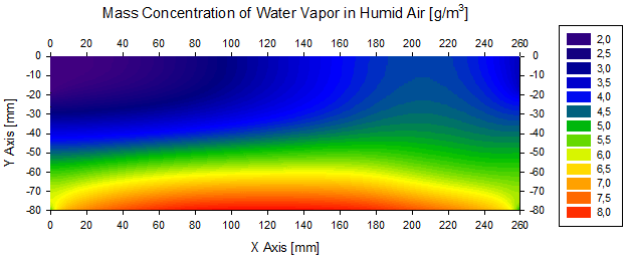

Figure 5. Mass concentration distribution of water vapor in humid air in the case of G=18mm after 10^6 iterations. (Figure is in color in the on-line version of the paper).

derived from temperature and mass concentration profiles are also given in Figure 6. Highest values near to the upper surface for vapor concentration, humidity ratio, and relative humidity have been performed within the length interval of 180-230 mm, where the effect of air inlet and outlet on the air flow has decreased. Near to the food load, where the relative humidity values have been near to the saturation conditions, maximum humidity ratio values have been ~6.5 g/kg. Average relative humidity and humidity ratio values have been 67.7% and 3.72 g/kg respectively.

Cumulative amount of surface condensation through the upper surface with respect to time is given in Figure 7. As seen in the contour graph, condensation occurs on the surface until ~90^{th} minutes after product loading. Surface condensation has occurred within the length interval of 40-180 mm, and had the maximum values within the length interval of 160-180 mm, where the effect of air inlet on the air flow has begun to decrease and humidity values has started to increase.

Numerical calculations were performed for cucumber being as the food load in the case of air inlet cross-section height being *G*=1 mm too. Air temperature distribution in the upper control volume CV1 and food load temperature distribution in the lower control volume CV2 after 10^6 iterations (1666 minutes) for the case of G=1mm are given in Figure 8 and Figure 9 respectively. Average temperature of the food load and maximum temperature near to the central region of the load have been 8.7°C and 10.6°C respectively, while the average air temperature has been 4.6°C. Because the pressure drop at the air outlet has been higher due to a smaller cross-section than the previous case, cold air flow has tended to collapse more in the air flow area. Hence, lower temperature values have been performed for the same air inlet velocity but smaller cross-section.

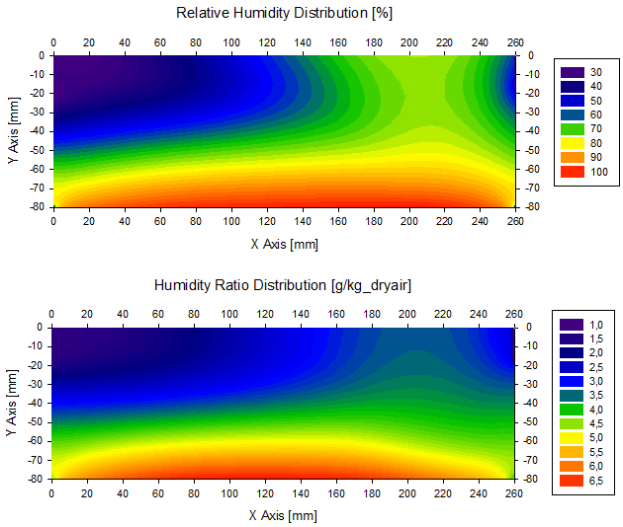

Figure 6. Relative humidity and humidity ratio distributions in the case of G=18mm after 10^6 iterations. (Figure is in color in the on-line version of the paper).

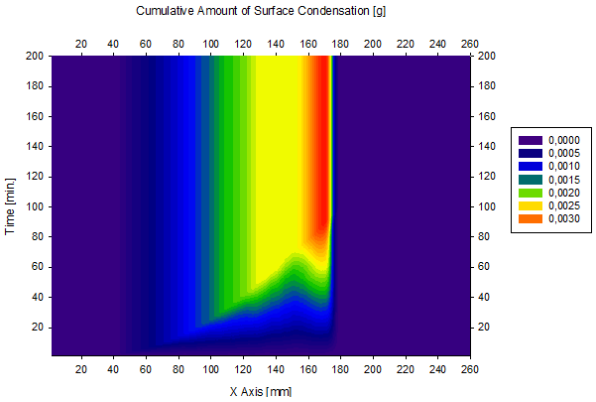

Figure 7. Cumulative amount of surface condensation with respect to time in the case of G=18mm after 10^6 iterations. (Figure is in color in the on-line version of the paper).

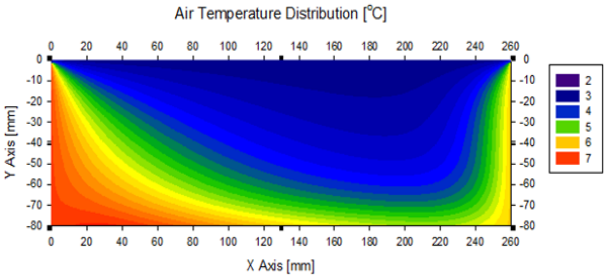

Figure 8. Air temperature distribution in the case of G=1mm after 10^6 iterations. (Figure is in color in the on-line version of the paper).

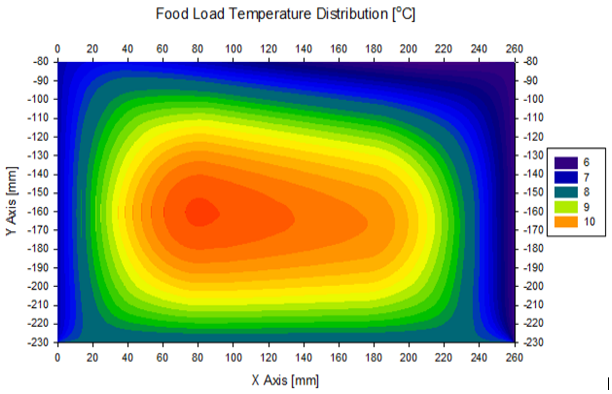

Figure 9. Food load temperature distribution in the case of G=1mm after 10^6 iterations. (Figure is in color in the on-line version of the paper).

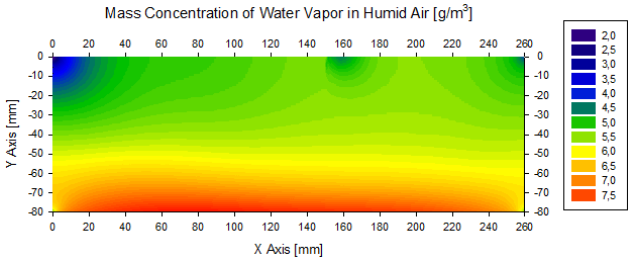

Figure 10. Mass concentration distribution of water vapor in humid air in the case of G=1mm after 10^6 iterations. (Figure is in color in the on-line version of the paper).

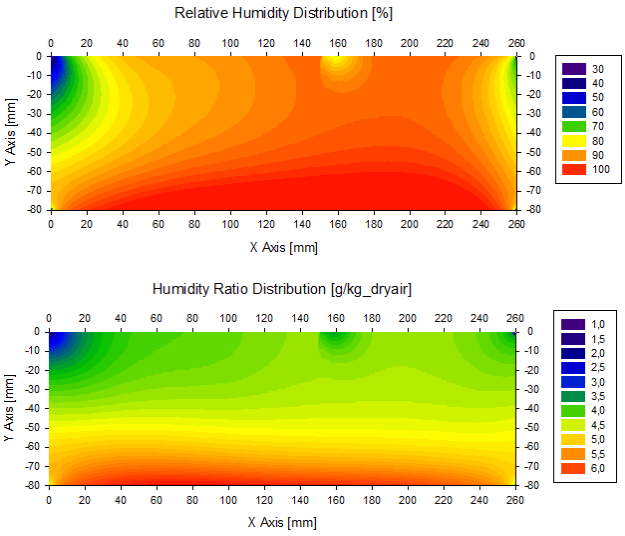

Figure 11. Relative humidity and humidity ratio distributions in the case of G=1mm after 10^6 iterations. (Figure is in color in the on-line version of the paper).

Mass concentration of water vapor in humid air after 10^6 iterations for the case of *G*=1mm is given in Figure 10. Relative humidity and humidity ratio distributions are also given in Figure 11. Average relative humidity and humidity ratio values have been 91.1% and 4.58 g/kg respectively. Because mass transport to the outside is lower due to smaller inlet-outlet cross sections, transpiration from the food has satisfied higher humidity values than the previous case. Total transpiration amounts from 4.5 kg cucumber surfaces have been calculated as 159 g and 134 g for the cases of *G*=18mm and *G*=1mm respectively. Due to higher relative humidity in the second case, moisture loss of the food has decreased ~16%. Surface condensation in the second case has also been ~4 times more than the second case due to higher humidity values in the space. In a real refrigerator case having two different crisper conditions having openings to perform approximate air inlet heights of *G*=18mm and *G*=1mm, an approximate 4-5 times surface condensation amount difference has been encountered. While the amount of surface condensation after 3 days storage in the first case has been 15-20 g, it has been 70-75 g in the second case.

Cumulative amount of surface condensation through the upper surface with respect to time for the second case is given in Figure 12. Different from the first case, surface condensation has continued during the whole storing period. Surface condensation has occurred within the length interval of 30-210 mm, which is a larger interval than the first case.

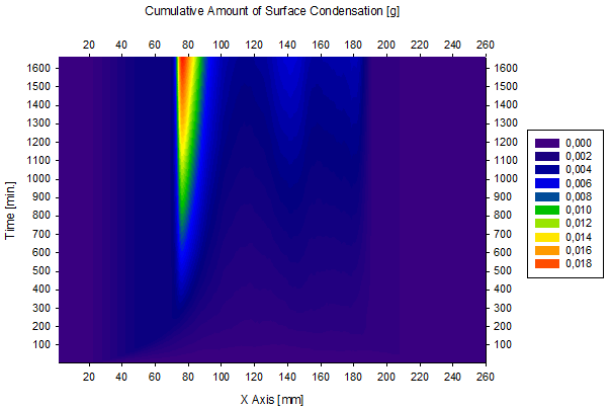

Figure 12. Cumulative amount of surface condensation with respect to time in the case of G=1mm after 10^6 iterations. (Figure is in color in the on-line version of the paper).

4. Conclusions

As the result of numerical simultaneous solution of transport equations for the two control volumes; temperature and humidity ratio distribution of the circulating humid air, temperature distribution within the food load, the amount of vapor transpiration from food products, and the amount of condensation on the underside of the upper surface were time-dependently determined. Numerical calculations were performed for cucumber being as the food load in the cases of air inlet cross-section height being *G*=18 mm and *G*=1 mm. Because mass transport to the outside is lower due to smaller inlet-outlet cross sections, transpiration from the food has satisfied higher humidity values than the previous case. Due to higher relative humidity in the second case, moisture loss of the food has decreased ~16%. Surface condensation in the second case has also been ~4 times more than the second case due to higher humidity values in the space. In *G*=18 mm case, condensation has occurred on the surface until ~90^{th} minutes after product loading, while it has continued during the whole storing period within a larger length interval in the *G*=1 mm case.

The amount of surface condensation under high humid conditions and difference between air and food load temperatures, show the necessity for modeling natural convection case. Because gravitational effects have been neglected in this study, mass concentration of water vapor near to the top surface and the amount of surface condensation tend to be lower than expected. Nevertheless, relative difference between the surface condensation amounts of two different cases (*G*=18mm and *G*=1mm) have been reasonable with regard to the representative

equivalent refrigerator crisper cases. For further study, numerical modeling for the natural convection case will also be held, and the results will be compared with the results of an experimental study that is planned to be performed simultaneous with numerical studies. While modeling natural convection case, gravitational effects due to temperature and concentration differences will also be taken into account in momentum equations. Because of relations between velocity distribution with temperature and concentration distributions in the natural convection case, momentum equations will need to be solved simultaneous with heat and mass transport equations.

Acknowledgements:

The authors would like to thank to colleagues and managers in Arçelik A.Ş. R&D Center, and Prof. Dr. Lütfullah Kuddusi and Asst. Prof. Dr. Melike Nikbay for their support in the PhD Thesis Committee in Istanbul Technical University.

Nomenclature

α	:	thermal diffusivity
c_x , c_y	:	dimensionless Courant numbers
c_p	:	specific heat
d_a	:	mass concentration of dry air
d_x , d_y	:	Dimensionless diffusivity numbers
d_v	:	mass concentration of water vapor
D_{va}	:	binary diffusion coefficient between air and water vapor
h	:	convective heat transfer coefficient
h_{fg}	:	phase change enthalpy
k	:	thermal conductivity
k_s	:	diffusive surface mass transfer coefficient
k_t	:	total transpiration coefficient
Λ	:	weight to surface area ratio
$\dot{m}_{CO2}$	:	CO_2 production rate
$m''_{cond.}$	:	surface condensation mass flux
$m''_{transp.}$	:	transpiration mass flux
Φ	:	relative humidity
P_s	:	water vapor saturation pressure on the surface
P_v	:	partial water vapor pressure in air
$q''_{resp.}$	:	heat of respiration
ρ	:	density
t	:	time
T	:	temperature
T_g	:	food (vegetable goods') temperature
u , v	:	velocity (horizontal, vertical)
υ	:	kinematic viscosity
ω	:	humidity ratio

References

Anderson, J. D. (1995). *Computational Fluid Dynamics: The Basics with Applications*. New York: McGraw-Hill.

ASHRAE Handbook (2006). *Refrigeration*, ASHRAE – American Society of Heating, Refrigerating and Air-Conditioning Engineers, Atlanta

Becker, B. R., Misra, A. ve Fricke, B. A. (1996). Bulk Refrigeration of Fruits and Vegetables Part 1: Theoritical Considerations of Heat and Mass Transfer, *HVAC&R Research*, Vol.***2***,* No.2, p.122-134.

Becker, B. R., Misra, A. ve Fricke, B. A. (1996). Bulk Refrigeration of Fruits and Vegetables Part 2: Computer Algorithm for Heat Loads and Moisture Loss, *HVAC&R Research*, Vol.***2***,* No.3, p.215-230.

Çengel, Y., and Boles, M, 2000, *Mühendislik Yaklaşımıyla Termodinamik*, Literatür Yayınevi, İstanbul

Incropera, F. P. ve DeWitt, D. P., trans. Derbentli et al. (2007). *Isı ve Kütle Geçişinin Temelleri*. İstanbul: Literatür Yayınları.

Mills, A. F. (2001). *Mass Transfer*. Upper Saddle River, NJ: Prentice Hall.

Olivieri, J., Singh, T. et al. (1996). *Psychrometrics: Theory and Practice*, ASHRAE – American Society of Heating, Refrigerating and Air-Conditioning Engineers, Atlanta, ABD.

Taner, D. J., Cleland, A. C., Opara, L. U. ve Robertson, T. R. (2002). A generalised mathematical modelling methodology for design of horticultural food packages exposed to refrigerated conditions Part 1: Formulation, *Int. J. Refrigeration*, Vol.***25***, p.33-42.

Taner, D. J., Cleland, A. C., Opara, L. U. ve Robertson, T. R. (2002). A generalised mathematical modelling methodology for design of horticultural food packages exposed to refrigerated conditions Part 2: Heat transfer modelling and testing, *Int. J. Refrigeration*, Vol.***25***, p.43-53.

Taner, D. J., Cleland, A. C., Opara, L. U. ve Robertson, T. R. (2002). A generalised mathematical modelling methodology for design of horticultural food packages exposed to refrigerated conditions Part 3: Mass transfer modelling and testing, *Int. J. Refrigeration*, Vol.***25***, p.54-65.

Terrell, W., Newell, T. A. (2007). Experimental techniques for determining heat and mass transfer due to condensation of humid air in cooled, open cavities, *Applied Thermal Engineering*, Vol.***27***, p.1574-1584.

Volchlov, E. P., Terekhov, V. V. ve Terekhov, V.I. (2004). A numerical study of boundary-layer heat and mass transfer in a forced flow of humid air with surface steam condensation, *Int. J. Heat and Mass Transfer*, Vol.***47***, p.1473-1481.

Wang, S., Chen, C. ve Yang, Y. (2006). Steady filmwise condensation with suction on a finite-size horizontal flat plate embedded in a porous medium based on Brinkman and Darcy models, *I. J. Thermal Sciences*, Vol.***45***, p.367-377.

White, A. J. (2000). Numerical investigation of condensing steam flow in boundary layers, *Int. J. Heat Fluid Flow*, Vol.***21***, p.727-734.

White, F. M. (1991). *Viscous Fluid Flow*. New York: McGraw-Hill.

Yang, Y., Chen, C. ve Hsu, P. (1997). Laminar film condensation on a finite-size horizontal wavy disk, *Applied Mathematical Modelling*, Vol.***21***, p.139-144.